Watershed rainfall forecasting using neuro-fuzzy networks with the assimilation of multi-sensor information

Fi-John Chang [a,*], Yen-Ming Chiang [b], Meng-Jung Tsai [a], Ming-Chang Shieh [c], Kuo-Lin Hsu [d], Soroosh Sorooshian [d]

[a] Department of Bioenvironmental Systems Engineering, National Taiwan University, Taipei, Taiwan
[b] Department of Hydraulic Engineering, Zhejiang University, Hangzhou, China
[c] Water Resources Agency, Ministry of Economic Affairs, Taipei, Taiwan
[d] Center for Hydrometeorology and Remote Sensing, Department of Civil and Environmental Engineering, University of California, Irvine, CA, USA

ARTICLE INFO

SUMMARY

The complex temporal heterogeneity of rainfall coupled with mountainous physiographic context makes a great challenge in the development of accurate short-term rainfall forecasts. This study aims to explore the effectiveness of multiple rainfall sources (gauge measurement, and radar and satellite products) for assimilation-based multi-sensor precipitation estimates and make multi-step-ahead rainfall forecasts based on the assimilated precipitation. Bias correction procedures for both radar and satellite precipitation products were first built, and the radar and satellite precipitation products were generated through the Quantitative Precipitation Estimation and Segregation Using Multiple Sensors (QPESUMS) and the Precipitation Estimation from Remotely Sensed Information using Artificial Neural Networks-Cloud Classification System (PERSIANN-CCS), respectively. Next, the synthesized assimilated precipitation was obtained by merging three precipitation sources (gauges, radars and satellites) according to their individual weighting factors optimized by nonlinear search methods. Finally, the multi-step-ahead rainfall forecasting was carried out by using the adaptive network-based fuzzy inference system (ANFIS). The Shihmen Reservoir watershed in northern Taiwan was the study area, where 641 hourly data sets of thirteen historical typhoon events were collected. Results revealed that the bias adjustments in QPESUMS and PERSIANN-CCS products did improve the accuracy of these precipitation products (in particular, 30–60% improvement rates for the QPESUMS, in terms of RMSE), and the adjusted PERSIANN-CCS and QPESUMS individually provided about 10% and 24% contribution accordingly to the assimilated precipitation. As far as rainfall forecasting is concerned, the results demonstrated that the ANFIS fed with the assimilated precipitation provided reliable and stable forecasts with the correlation coefficients higher than 0.85 and 0.72 for one- and two-hour-ahead rainfall forecasting, respectively. The obtained forecasting results are very valuable information for the flood warning in the study watershed during typhoon periods.

© 2013 Elsevier B.V. All rights reserved.

1. Introduction

Rainfall is a key hydrological variable that links the atmosphere and land surface processes. The complex temporal heterogeneity of typhoon rainfall coupled with mountainous physiographic context makes the development of accurate forecasting reservoir inflow several hours ahead of time a great challenge. Typhoons are commonly coupled with heavy rainfall. For instance, the highest rainfall record of Typhoon Morakot was over 1000 mm/day in southern Taiwan in 2009. Due to abundant rainwater, the inundation disaster occurred in most of this area and caused more than

USD 0.5 billion losses. The fatally rainfall-induced landslide buried the entire Shaoling village, which killed about 500 people in the village alone. Consequently short-term typhoon rainfall forecasting is recognized as the most important study for reservoir watershed management and flood mitigation in Taiwan. As far as rainfall forecasting is concerned, the accuracy of precipitation products and their nowcasting is continuously improved and becomes more reliable for practical applications in recent years. For example, Kober et al. (2012) blended a probabilistic nowcasting method with a high-resolution numerical weather prediction assimilated for convective precipitation forecasts. Haiden et al. (2011) presented the integrated nowcasting through a comprehensive analysis system and provided the products of precipitation amount and types. Sokol (2006) applied a multiple linear regression model

---

complemented by a correction procedure for nowcasting of 1-h precipitation using radar and numerical weather prediction data. Sokol and Pesice (2012) proposed a model SAM for nowcasting 1 to 3-h precipitation totals and improved forecasts accuracy. Zahraei et al. (2012) introduced a pixel-based algorithm for short-term quantitative precipitation forecasting using radar-based rainfall data and shown promising performance in severe storms forecasting.

Precipitation observations, in general, are available from several sources, such as ground rain gauges, radars and satellites. These sources not only have significant differences in both spatial and temporal resolutions but also have different limitations subject to hardware mechanisms. Ground gauges observe surface precipitation continuously and directly, however, gauges are sparsely located and only provide point-scale measurements, which imply the spatial representation of gauges is weak. Radars use reflected microwave energy to derive precipitation at a height between about 500 m and 5000 m above sea level, however, radar coverage is many times limited by orography. Satellites, whose coverage is not limited by orography, provide rapid precipitation information over large areas. However, satellite measurements not only are indirectly related to surface precipitation but also have lower spatial and temporal resolutions, as compared to those of radar products. On account of the different strengths and weaknesses of each measurement technology, a potential advantage is thereby to integrate precipitation measurements from different measurement apparatuses such as gauges, radars and satellites for improving the accuracy of rainfall forecast (Grecu and Krajewski, 2000; Kidd et al., 2003; Chiang et al., 2007a; Mittermaier, 2008).

The Artificial Neural Network (ANN) was inspired by neurobiology to perform brain-like computations and has been recognized as an effective tool for modeling complex nonlinear systems in the last two decades. The applications of ANNs to various aspects of hydrological modeling have provided many promising results, such as rainfall estimation/prediction (Hong et al., 2005, 2006; Chiang et al., 2007a; Chen et al., 2011), flood forecasting (Chiang and Chang, 2009; Siou et al., 2011; Yilmaz et al., 2011), and water level prediction (Chiang et al., 2010; Adamowski and Chan, 2011). Neuro-fuzzy systems that combine ANNs and fuzzy theories have proven to be another powerful intelligent system and have received much attention in recent years (Chang et al., 2005; Coulibaly and Evora, 2007; Firat, 2008; Lohani et al., 2011). Both ANNs and fuzzy theories have been developed to simulate the thinking process of human brain for learning similar strategies or experiences to make optimal decisions. Nevertheless, the fundamental mechanisms of these two theories are different, in which ANNs offer a superior capability to extract significant features from complex databases and are capable of learning the relationship between any data pairs, whereas the fuzzy logic is based on the way how brains deal with inexact information. Due to the lack of learning capability for fuzzy theories, it is difficult to tune the fuzzy rules and membership functions based on training data. Therefore, the neuro-fuzzy system was developed for capturing the advantages and strengths of both ANNs and fuzzy logic in a single framework. The adaptive network-based fuzzy inference system (ANFIS), proposed by Jang (1993), is one of the famous neuro-fuzzy systems and has been applied to modeling daily discharge responses (Kurtulus and Razack, 2010), water level prediction (Chiang et al., 2011), and rainfall-runoff simulations (Shu and Ouarda, 2008).

This study aims at providing reliable and accurate short-term typhoon rainfall forecasts using artificial intelligent (AI) techniques based on the assimilation of satellite- and radar-derived rainfall estimations and ground gauge measurements. The organization of this paper is addressed as follows. The description of the study area, ground measurements, radar-derived and satellite-derived precipitation estimation as well as the model construction is provided in Section 2. Section 3 presents the methodologies, including the back-propagation neural network (BPNN) for bias adjustment, the genetic algorithm (GA) for data merge, and the ANFIS for rainfall forecasting. Section 4 shows the results and comparison of two bias correction strategies, the effectiveness of merging precipitation products, and the performance of rainfall forecasting. Finally, the conclusions are given in Section 5.

2. Materials

2.1. Study area and gauging station datasets

The study area of this study belongs to the Shihmen Reservoir watershed and is located on the upstream of the Tahan River in northern Taiwan. Fig. 1 shows the locations of the Shihmen Reservoir watershed where the reservoir inflow gauging station is denoted with a blue[1] star, each radar station is denoted with a purple square, and each of thirteen rain gauging stations is denoted with a red dot. All the thirteen rain gauging stations are spatially well distributed below 2000 m in elevation. Under this condition, no rain gauge is set up above 2000 m. Alternatively, remote sensing, such as radar and satellite, is considered to provide rainfall information for areas above 2000 m. This watershed receives an annual rainfall of about 2500 mm, which mainly comes from typhoons. Because rainwater usually occurs in a short duration with great intensity, heavy rainfall coupled with huge runoff would flows into the Reservoir in just a couple of hours. Consequently, reliable typhoon rainfall forecasting plays an important role in reservoir operation and management because typhoons usually affect Taiwan for about 3–5 days. Four types of data, including reservoir inflow (m^3/s), rain gauge measurements (mm), and radar- and satellite-derived precipitation estimations (mm) were collected from 2006 to 2009 in this study. A total of 641 hourly data associated with thirteen historical typhoon events were obtained.

2.2. Radar-derived precipitation datasets

The radar-derived precipitation estimation applied in this study can be referred to the QPESUMS (Quantitative Precipitation Estimation and Segregation Using Multiple Sensors) system (http://qpesums.cwb.gov.tw/taiwan-html2/), which was developed by the Central Weather Bureau (CWB) of Taiwan and the National Severe Storms Laboratory (NSSL) of National Oceanic and Atmospheric Agency (NOAA) of the USA. The QPESUMS system mainly composes of four weather Doppler radars that cover the whole of Taiwan and the adjacent ocean, and it records base reflectivity with a spatial resolution of 0.0125° in both longitude and latitude and a temporal resolution of 10 min. The R_1 radar station has the shortest distance to the study area (less than 80 km) and is located at longitude 121.46°E and latitude 25.04°N with an elevation of 760 m. This radar belongs to the Weather Surveillance Radar 1988 Doppler (WSR-88D) with a wavelength of 10 cm (S-band) and performs approximately 10 different elevation scans (between 0.5° and 15° above the horizon) that consist of a complete volume scan. The beam width is 0.857°. The system generates the constant altitude plan position indicators (CAPPI) at the elevation of 1000 m and estimates rainfall using the Z–R relation with the function type $Z = 32.5R^{1.65}$. Therefore, the records of 434 grid pixels are collected to cover the whole of the watershed for every 10 min. Even though the QPESUMS system is used to monitor rainfall in Taiwan, the Z–R relationship for converting radar reflectivity to rainfall rates can be affected by various problems, such as ground clutter and beam

---

[1] For interpretation of color in Figs. 1 and 5, the reader is referred to the web version of this article.
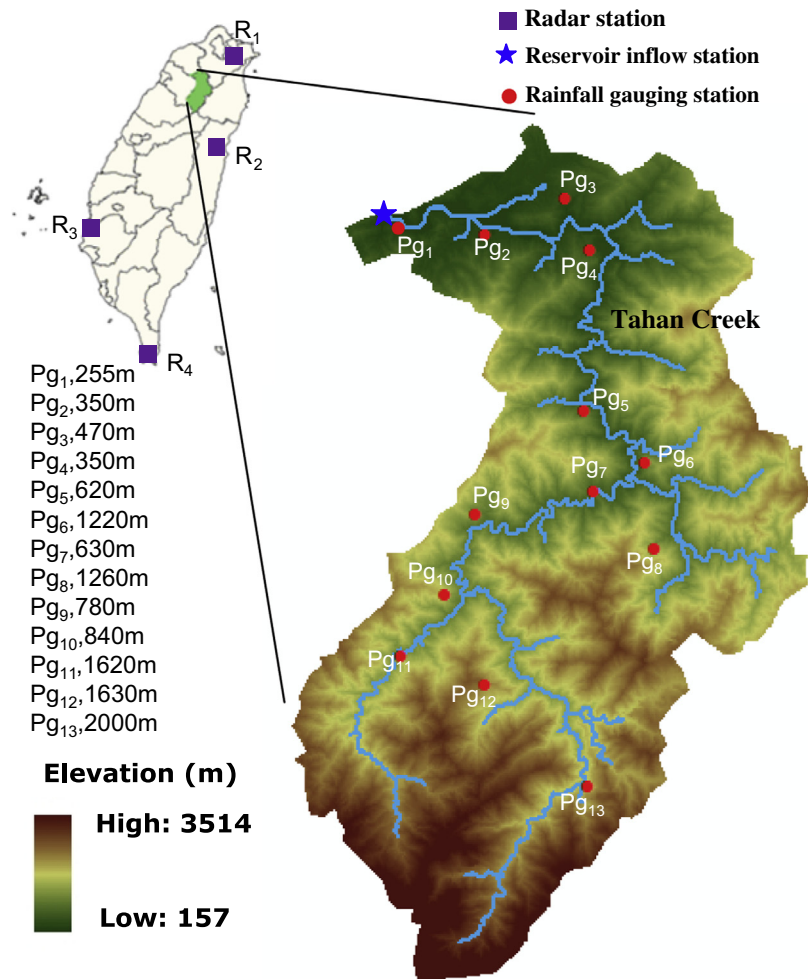
Fig. 1. Locations of the study area, rainfall gauging stations, radar stations and the Tahan Creek and its upstream tributaries.

blockage. Due to various limitations on the radar scan range, less forecast precision is expected in the mountainous areas at higher elevations in Taiwan (Chen et al., 2007). Besides, the function type of the *Z–R* relationship may vary from place to place or from weather type to weather type (Chiang et al., 2007a).

2.3. Satellite-derived precipitation datasets

The satellite-derived precipitation estimation used in this study comes from the PERSIANN-CCS (Precipitation Estimation from Remotely Sensed Information using Artificial Neural Networks-Cloud Classification System), proposed by Hong et al. (2004), which has been widely applied to rainfall estimations in recent years (Juglea et al., 2010). The system uses the infrared images of global geosynchronous satellites (GOES, MTSAT, and Meteosat) to generate 30-min rain rates (in this case study, satellite data mainly came from the MTSAT launched by Japan). Long wave infrared images (10.7 μm) are first extracted from these satellites. In contrast with traditional constant threshold approaches, the PERSIANN-CCS applies a variable threshold to the cloud segmentation so that the system is able to identify individual cloud-patches. Then, an individual cloud-patch can be further classified according to its geometric properties, texture, dynamic evolution and the height of the cloud top. These classifications help in converting precipitation values to pixels within each cloud-patch based on a specific curve describing the relationship between rain-rate and temperature. Model parameters are regularly updated using rainfall estimates from the Next-

Generation Weather Radar (NEXRAD) network. The PERSIANN-CCS provides precipitation estimations with a spatial resolution of 0.04° and a temporal resolution of 30 min, and therefore 45 grid pixels of PERSIANN-CCS products are collected every half an hour, which are sufficient to cover the whole of the watershed in this study. Even though satellite data are not affected by topography and can be used to measure rainfall over a large area, the PERSI-ANN-CCS usually underestimates rainfall during typhoon periods (Chiang et al., 2007b).

2.4. Data preprocessing and configuration

Based on the above description, there is a necessity of introducing a bias correction procedure to adjust both QPESUMS and PER-SIANN-CCS precipitation estimations in order to reliably realize the contribution of radar and satellite information to the merging process of precipitation products at mountainous areas. Moreover, it is important to match different precipitation sources in both spatial and temporal resolutions. To investigate the effectiveness of the proposed merging process, this study simply converts all precipitation products to the same spatial and temporal resolutions, that is, hourly average precipitation over the basin. The average precipitation over the basin based on gauge measurements is calculated by the Thiessen method while those based on both QPESUMS and PERSIANN-CCS products are calculated by the weighted average of all pixels.

As for the configuration of thirteen typhoon events, 7 events with 350 hourly data were arranged in the training phase for calibrating the model structure and parameters, 3 events with 153 hourly data were arranged in the validation phase for determining the training epochs in order to avoid over-fitting problems, and the remaining 3 events with 138 hourly data were arranged in the testing phase for evaluating the performance and generalization capability of the determined network. Table 1 shows the statistics of these three independent datasets.

3. Methodology

A novel approach that comprises two main parts is proposed: (1) the bias correction and the assimilation of multi-sensor rainfall information using the BPNN and the GA, respectively; and (2) the construction of multi-step-ahead rainfall forecasting through the ANFIS. The first part is mainly to explore the effectiveness of assimilating multiple rainfall sources (satellite precipitation product, radar precipitation product and ground gauge measurements), and the second part intends to provide reliable and accurate 1–2 h-ahead rainfall forecasts based on the assimilated precipitation. Fig. 2 illustrates the schematic flowchart of this study. The detailed procedures and a brief introduction of the implementation methods, i.e., BPNN and ANFIS, are given as follows:

3.1. Back-propagation neural network (BPNN)

The BPNN is widely used for hydrological modeling and has received numerous successes in simulations and predictions. The BPNN has unique advantages such as the excellent convergence capability. The steepest descent method is one of the algorithms that are frequently adopted for training the BPNN, but, however, it often suffers from local optimizations. To overcome this problem, the conjugate gradient algorithm has now become much popular because it represents a compromise between the simplicity of the steepest descent method and the fast quadratic convergence of the Newton's method. In general, the conjugate gradient algorithm makes a good uniform progress toward the solution at each step and has been found to be effective in searching a better solution than the steepest descent method (Haykin, 1999; Chiang et al., 2004). Therefore, the conjugate gradient algorithm was applied in this study for model calibration.

3.2. Adaptive network-based fuzzy inference system (ANFIS)

The ANFIS has received much attention because of its outstanding capability of learning any real continuous function. The ANFIS not only maintains the learning ability of ANNs for mapping an input space onto an output space but also possesses the advantages of fuzzy if-then rules for describing the local behavior of such mapping. The system results can then be obtained through the reasoning capability of fuzzy logics. The architecture of the ANFIS consists of five layers, and the training of the ANFIS can be referred to a hybrid learning algorithm, that is, an incorporation of the gradient descent method and the least-squares method. Furthermore, the determination of the number of fuzzy rules is an important step when applying the ANFIS. When the number of rules increases, the number of parameters determined will become enormous, which will consume considerable computational time and, even worse, result in decreasing the capability of generalization. To solve this problem, the fuzzy subtractive clustering algorithm is adopted for establishing the relationship between input and output variables. The fuzzy subtractive clustering algorithm can effectively distinguish the fuzzy qualities associated with each of the clusters through the minimum number of rules. Details of the ANFIS modeling with the fuzzy subtractive clustering can be found in Chang and Chang (2001).

3.3. BPNN modeling for bias corrections

According to the correlation analysis between reservoir inflow and all rain gauges at different lag times, it suggested that the time of concentration in the study area was about 5–7 h. Nevertheless, the inflow prediction could merely be performed at a lead time of 5 h only if observations were available. In other words, rainfall forecasting at lead times of 1 and 2 h should be provided if the inflow prediction is required for a lead time of 7 h. Eq. (1) shows the relationship between rainfall and inflow when constructing the rainfall–runoff model.

$$Y(t+n) = f(X_g(t+n-5), X_g(t+n-6), X_g(t+n-7)) \qquad (1)$$

where Y and X_g denote reservoir inflow and rain gauge measurements, respectively. The $f()$ is a nonlinear transfer function, i.e., a sigmoid function, and t and n are current time and forecast lead time, respectively.

To correct the bias of each precipitation product, the BPNN was used to find the nonlinear function. Two independent BPNNs were separately fed with uncorrected QPESUMS and PERSIANN-CCS precipitation data for fitting the ground gauge values of training datasets. As far as the model setting was concerned, the BPNN consisted of three layers: an input layer with a single input (QPESUMS or PERSIANN-CCS precipitation data); a hidden layer with hidden nodes determined by trial-and-error (usually less than 5 nodes); and an output layer with a single output (corrected rainfall (X')). The optimization/stop criteria included the minimal error (0.0001 mm/h) and the number of learning iterations (1000). The model optimization procedure would stop when reaching either of the two criteria. Because the direct outputs of the model might not provide a meaningful representation as compared with those of the original QPESUMS and PERSIANN-CCS precipitation products, it was necessary to specifically present the biases and random errors of the original QPESUMS and PERSIANN-CCS precipitation products. Therefore, coefficients a and b were assumed for the purpose of transforming the BPNN outputs into the following formats:

$$X'_r(t) = a_1 X_r(t) + b_1 \qquad (2)$$

$$X'_s(t) = a_2 X_s(t) + b_2 \qquad (3)$$

where X'_r and X'_s represent the corrected radar and satellite products (BPNN outputs), respectively. a and b represent the random and bias errors of uncorrected (original) radar and satellite precipitation products (X_r and X_s, respectively).

The bias correction procedure consisted of two modules (area to area (A–A) and point to point (P–P) modules), which investigated the influence of spatial resolution of rainfall on the bias correction. The A–A module meant that the bias correction was performed with a basin-scale average precipitation product. In other words, the A–A module simply calculated the average precipitation over the basin based on the QPESUMS (or PERSIANN-CCS) products

Table 1
Statistics of ground precipitation measurements in different datasets.

	Event ([a])	Max.	Min.	Mean[b]	SD[c]
Training	7 (350)	44.4	0	6.5	8.2
Validation	3 (153)	33.2	0	4.3	6.2
Testing	3 (138)	26.9	0	5.1	6.2

[a] Number of data.
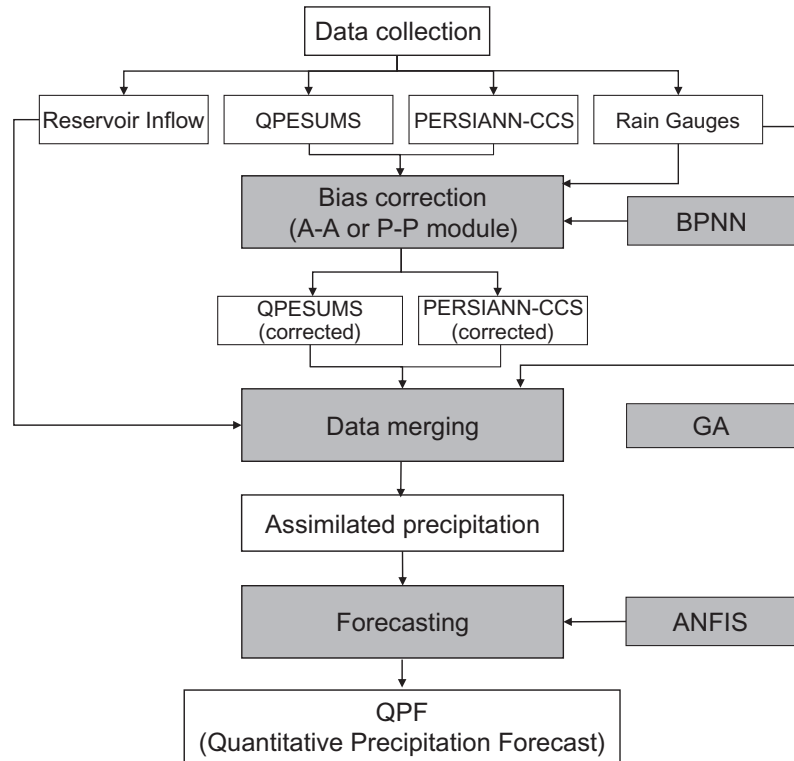[b] Unit (mm/h).
[c] Standard deviation.

Fig. 2. Flowchart of this study.

through the weighted average method, and then the BPNN was constructed for correcting the biases of the QPESUMS (or PERSI-ANN-CCS) precipitation product. Alternatively, the P–P module meant that the bias adjustment was first carried out for the selected 13 grid pixels right above each 13 ground rain gauging stations, and then the remaining pixels were corrected by using the inverse distance weighting (IDW) method based on the 13 adjusted pixels. The IDW method was used to correct the precipitation value X at the location of the remaining pixels P_o, given the adjusted precipitation values X' at the location of 13 adjusted pixels P_i. The procedure is shown as flows:

$$X(P_o) = \sum_{i=1}^{n} \lambda_i X'(P_i) \tag{4}$$

where $n = 13$ in this case; λ_i represents the weights that are calculated from the distances between the adjusted pixels (P_i) and the remaining pixels (P_o) and can be defined as follows:

$$\lambda_i = \frac{f(d_{oi})}{\sum_{i=1}^{n} f(d_{oi})} \tag{5}$$

where f represents the inverse square ratio as shown in Eq. (6):

$$f(d_{oi}) = \frac{1}{d_{oi}^2} \tag{6}$$

where d_{oi} is the distance between P_o and P_i.

3.4. Precipitation merging process

After conducting the bias correction, the GA was implemented to search the optimal weighting factors that represent the contribution of different precipitation products to the merging process. The GA is a common and popular optimization technique that can efficiently search the whole parameter domain to find the best parameter set that minimizes the objective function. This algo-

rithm enjoys a widespread use and can be found in many previous studies (Chiu et al., 2007; Li and Shao, 2010). The assimilated precipitation was expected to be obtained through the optimization process of the GA. The objective function (F) and the constraint designed in this study for the precipitation merging process are listed as follows:

$$Min(F) = \min\left\{ \sqrt{\frac{\sum [f(X_g(t-5) \times \theta_1 + X'_r(t-5) \times \theta_2 + X'_s(t-5) \times \theta_3) - Y(t)]^2}{N}} \right\} \tag{7}$$

$$\text{Two types of constraints}: \quad \theta_1 + \theta_2 + \theta_3 \\ \leqslant 1 \text{ or } \theta_1 + \theta_2 + \theta_3 = 1 \tag{8}$$

where θ_1, θ_2, and θ_3 represent the corresponding merging weighting factors; $f()$ is the nonlinear sigmoid function; and Y and X_g, X'_r and X'_s represent reservoir inflow, rain gauge measurement, corrected radar product and corrected satellite product, respectively.

3.5. ANFIS modeling for short-term rainfall forecasts

To further demonstrate the effectiveness of the assimilated precipitation, two input scenarios were constructed and implemented through the ANFIS models for one- and two-hour-ahead rainfall forecasting. The input dimension of scenario 1 is three (rain gauge, and corrected QPESUMS and PERSIANN-CCS precipitation products); whereas the input dimension of scenario 2 is one (the assimilated precipitation). The type of the membership functions used in the ANFIS models for both scenarios is the Gaussian function, and a total of five membership functions are determined after model training. For each scenario, two ANFIS models are separately constructed for one- and two-hour-ahead rainfall forecasting. The model optimization procedure will be stopped when reaching either the minimal error or the maximal learning epoch.

3.6. Evaluation criteria

Several statistical criteria were selected for evaluating the model performance. The agreement between observations and forecasts was calculated based on correlation coefficient (CC), root mean square error (RMSE), normalized root mean square error (NRMSE), and mean absolute error (MAE). The RMSE is used as a common performance measure and usually results in larger errors that occur in the vicinity of high flows in general; whereas the MAE computes all deviations from the original data series and is not weighted towards high values. A skill score (SS) was also used for evaluating the percentage improvement in any target model with respect to a reference model. These criteria are defined as follows:

$$CC = \frac{\sum_{i=1}^{N}(X(i) - \overline{X})(\widehat{X}(i) - \overline{\widehat{X}})}{\sqrt{\sum_{i=1}^{N}(X(i) - \overline{X})^2 \sum_{i=1}^{N}(\widehat{X}(i) - \overline{\widehat{X}})^2}} \quad (9)$$

$$RMSE = \sqrt{\frac{\sum_{i=1}^{N}(\widehat{X}(i) - X(i))^2}{N}} \quad (10)$$

$$NRMSE = \frac{1}{\sigma}\sqrt{\frac{\sum_{i=1}^{N}(\widehat{X}(i) - X(i))^2}{N}} \quad (11)$$

$$MAE = \frac{\sum_{i=1}^{N}\left|(\widehat{X}(i) - X(i))\right|}{N} \quad (12)$$

$$SS = \left(\frac{E_{RM} - E_{TM}}{E_{RM}}\right) \times 100\% \quad (13)$$

where $\widehat{X}$ is the estimated rainfall (mm/h), X is the observed rainfall (mm/h), and $\overline{X}$ and $\widehat{X}$ are the mean of observed and estimated rainfall, respectively. σ is the standard deviation. E_{TM} and E_{RM} are the statistical error measurements in any target and reference models, respectively. For rainfall forecasting, the target and reference models were the ANFIS models fed with input scenarios 2 and 1, respectively. A positive SS indicates the performance of the model fed with input scenario 2 is better than that of input scenario 1.

4. Results and discussion

4.1. Bias corrections for QPESUMs and PERSIANN-CCS products

Fig. 3 shows the observational data and the bias correction results performed in the QPESUMS precipitation product. The brown histogram indicates the gauge observations, the red line indicates the original QPESUMS precipitation product, and the blue line means the corrected QPESUMS precipitation product. It is obvious that the original QPESUMS precipitation product signifi-
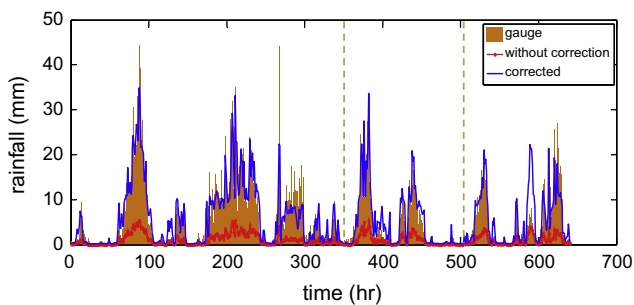

Fig. 3. Comparison of gauge measurements and QPESUMS precipitation products with (A–A module) and without a bias correction (training: hour 1–350; validation: hour 351–503; and testing: hour 504–641).

cantly underestimated precipitation due to parts of the radar detection was blocked by mountains. Besides, the QPESUMS only applied a single Z–R power-law function to estimating the precipitation of the whole Taiwan, which might not effectively represent the spatial distribution of precipitation. It is known that the optimal parameters in the Z–R power-law function are "scale dependent" (Morin et al., 2003) and they may vary from place to place and from season to season (Chiang et al., 2007a). Therefore, a low precision of the QPESUMS precipitation product is expected.

Table 2 illustrates the performance of the bias correction (A–A module) in QPESUMS and PERSIANN-CCS precipitation products by using the BPNN and regression models, respectively. It appears that the QPESUMS gains great improvement in terms of much lower RMSE, NRMSE and MAE values than those of the uncorrected QPESUMS. For instance, the values of RMSE in all three phases (i.e., training, validation and testing) of the BPNN are significantly dropped: from 8.8 to 3.3 (training); from 6.2 to 2.4 (validation); and from 6.8 to 4.2 (testing). We also notice that the results obtained from the BPNN are slightly better than those of the regression methods. The results shown in Fig. 3 and Table 2 clearly indicate that the proposed bias corrections (via the BPNN or regression methods) in the QPESUMS precipitation product can largely mitigate the underestimation problem of the product and effectively increase the product accuracy. The corrected QPESUMS precipitation is close to ground observations except for few peak values.

The bias corrections performed in A–A module by both BPNN and regression methods also brought positive effects on the PERSIANN-CCS even though the improvement was not as much as that of the QPESUMS. This could be in consequence of model calibration because the parameters of PERSIANN-CCS were mainly calibrated according to the continental climate (rainfall intensity is in general less than 10 mm/h), which is rather different from the subtropical climate of an island such as Taiwan (rainfall intensity can easily achieve 20 mm/h during typhoon periods). Therefore, the precipitation product generated by PERSIANN-CCS systematically underestimated precipitation, particularly for rainfall intensity over 10 mm/h, and thus failed to well capture the precipitation trend (see Fig. 4). Besides, we notice that even though the results of the regression-based bias correction for the PERSIANN-CCS are better than those of the BPNN-based one in the training phases, the performances of the regression-based bias correction in both validation and testing phases are even worse than the original (uncorrected) precipitation products (see Table 2). This finding demonstrates that the linear regression model is capable of dealing with data that have a significant correlation (rain gauge and QPESUMS), but, however, it is not able to handle scattered or irregular data (PERSIANN-CCS).

Table 3 indicates the improvement rates of the corrected QPESUMS and PERSIANN-CCS precipitation products at 13 gauging sites through the P–P module. The performance is similar to that of the A–A module: the accuracy of the QPESUMS can be considerably enhanced whereas the precision of the PERSIANN-CCS is slightly improved only. The improvement rates, in terms of RMSE, for the QPESUMS obtained from the A–A and P–P modules in the testing phases are 38% and around 30–60% (for the thirteen gauging stations), respectively. The results indicate that the bias correction through the P–P module, in general, performed better than that of the A–A module. This result conforms to the fact that the A–A module only uses one reference (basin-scale average precipitation calculated from 13 ground gauging stations) for bias correction, whereas the P–P module uses observational data obtained from 13 ground gauges for the same task. We also notice that the improvement rates of the corrected QPESUMS for those gauged sites close to the reservoir (i.e., Pg_1–Pg_4) are, in general, much
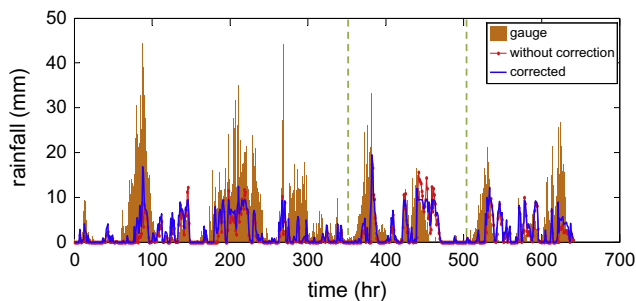
Table 2
Performance of the bias corrections (A–A module) in QPESUMS and PERSIANN-CCS precipitation products through the BPNN and regression models.

Correction	QPESUMS			PERSIANN-CCS		
	Before	BPNN	Regression	Before	BPNN	Regression
Training						
RMSE[a]	8.8	3.3	3.4	8.7	8.4	7.1
NRMSE[a]	1.08	0.40	0.42	1.07	1.03	0.87
MAE[a]	5.4	2.0	2.1	5.4	5.2	5.3
Validation						
RMSE	6.2	2.4	2.6	6.6	6.5	8.5
NRMSE	0.99	0.39	0.43	1.07	1.05	1.37
MAE	3.4	1.6	1.6	3.9	3.8	6.5
Testing						
RMSE	6.8	4.2	4.4	7.2	6.9	7.4
NRMSE	1.09	0.67	0.70	1.15	1.11	1.18
MAE	4.1	2.4	2.5	4.7	4.8	5.9

[a] Unit (mm/h).

Fig. 4. Comparison of gauge measurements and PERSIANN-CCS precipitation products with (A–A module) and without a bias correction (training: hour 1–350; validation: hour 351–503; and testing: hour 504–641).

Table 3
Improvement rates of the corrected QPESUMS and PERSIANN-CCS precipitation products (P–P module) at 13 rain gauge stations in the testing phase.

	RMSE		MAE	
	QPESUMS (%)	PERSIANN-CCS (%)	QPESUMS (%)	PERSIANN-CCS (%)
Pg_1	60.3	3.2	60.8	5.1
Pg_2	52.1	1.9	43.8	1.1
Pg_3	51.3	0.5	49.5	0.3
Pg_4	54.1	2.7	52.7	0.9
Pg_5	30.8	1.5	22.9	0.8
Pg_6	51.5	2.0	51.9	-0.2
Pg_7	47.3	0.1	47.5	1.3
Pg_8	51.7	1.1	52.0	1.0
Pg_9	43.6	1.8	44.4	0.7
Pg_{10}	41.8	2.8	43.6	1.5
Pg_{11}	31.8	1.8	37.3	2.3
Pg_{12}	44.0	3.3	44.4	1.6
Pg_{13}	35.6	1.9	31.8	0.1

higher than those of the upstream gauged sites (i.e., far from the reservoir, Pg_9–Pg_{13}).

After conducting bias corrections, we found that the precision of the PERSIANN-CCS was slightly improved only and the improvement rates of the OPESUMS in P–P module were larger for gauges at lower elevations than those at higher elevations. The counter-measures to those phenomena can be further explored in future work for improving the precision of the remote-sensing precipitation products.

4.2. Assimilation of multiple precipitation sources

Even through the bias correction of the PERSIANN-CCS is not significant, the PERSIANN-CCS precipitation product may has

Table 4
Optimal merging weighting factors for different precipitation products derived from the GA and least square method (LSM), and the comparison of ground measurements and the assimilated precipitation in terms of RMSE.

$\theta_1 + \theta_2 + \theta_3 \leqslant 1$[a]	Module	θ_1	θ_2	θ_3	Testing performance (RMSE[b])
GA	A–A	0.59	0.29	0.06	615
	P–P	0.56	0.30	0.06	613
LSM	A–A	0.56	0.30	0.07	615
	P–P	0.56	0.30	0.07	613
$\theta_1 + \theta_2 + \theta_3 \leqslant 1$					
GA	A–A	0.79	0.14	0.07	622
	P–P	0.66	0.24	0.10	619
LSM	A–A	0.69	0.25	0.06	620
	P–P	0.69	0.23	0.08	619

[a] θ_1, θ_2, θ_3 represent the merging weighting factors corresponding to rain gauge measurement, corrected radar product and corrected satellite product, respectively.
[b] Unit (m^3/s).

potential advantages on data merging because the mechanisms between the radar and satellite detection are distinguishing. Besides, the radar coverage could be limited or affected by topography because the study area belongs to a mountainous watershed. Moreover, the spatial representation of ground gauges is low, and, in particular, no rain gauging station is located above 2000 m in the study area. As for satellite images, they are not limited by topography and are able to provide rapid measurements over large areas. In other words, information comes from satellites may possess important precipitation characteristics that may not be captured by radars or ground gauges. Therefore, the gauge, radar and satellite information were taken into consideration for precipitation merging in this study. Two nonlinear optimization search methods, i.e., the GA and the least square method (LSM), were conducted to search the optimal merging weighting factors through minimizing Eq. (7).

Table 4 shows the optimal merging weighting factors of the assimilated precipitation obtained from the GA and the LSM, in which the optimal value of a merging weighting factor represents the contribution percentage of the corresponding precipitation source over the assimilated precipitation. Basically, both GA and LSM produced similar results (similar weighting factors and performance) under the same conditions. In the present study, the individual contribution of rain gauge measurements, QPESUMS and PERSIANN-CCS information to the assimilated precipitation subject to the constraint of $\theta_1 + \theta_2 + \theta_3 = 1$ was 69–79%, 14–25% and 6–7% accordingly when the A–A module was applied, whereas
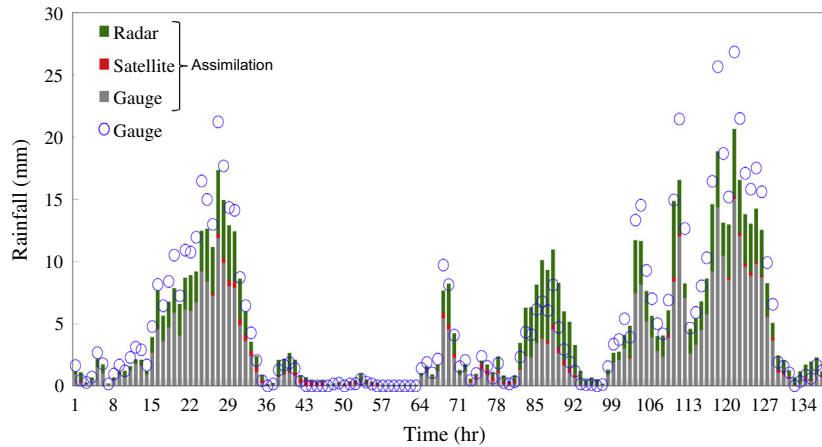
Fig. 5. Contribution of gauge, radar and satellite precipitation products to the assimilated precipitation (A–A module).

Table 5
Comparison of rainfall forecasts obtained from the A–A module-based scenarios 1 and 2.

	Scenario 1[a]			Scenario 2[b]					
	ANFIS			ANFIS			Regression		
	Training	Validation	Testing	Training	Validation	Testing	Training	Validation	Testing
t + 1									
CC	0.85	0.80	0.71	0.88	0.85	0.85	0.83	0.84	0.83
RMSE[c]	4.33	4.12	4.70	3.88	3.52	3.37	4.55	3.54	3.45
MAE[c]	2.65	2.56	3.07	2.39	2.00	2.23	2.81	2.29	2.36
t + 2									
CC	0.77	0.74	0.61	0.78	0.79	0.72	0.72	0.74	0.69
RMSE	5.21	4.53	5.29	5.05	4.02	4.43	5.67	4.41	4.49
MAE	3.32	2.92	3.77	3.14	2.65	3.15	3.63	3.05	3.38

[a] Inputs: rain gauge, QPESUMS, and PERSIANN-CCS precipitation.
[b] Input: assimilated precipitation.
[c] Unit (mm/h).

66–69%, 23–24% and 8–10% accordingly when the P–P module was used. When under the constraint of $\theta_1 + \theta_2 + \theta_3 \leqslant 1$, the optimal weighting factors were more consistent for both A–A and P–P modules no matter which search method was used.

According to the performance obtained from these two types of constraints, it shows that a lower RMSE value could be gained when the constraint of $\theta_1 + \theta_2 + \theta_3 \leqslant 1$ was given. We notice that the sum of the optimal weighting factors is less than 0.95 for all

cases, which could result in the underestimation of the assimilated precipitation. This phenomenon implies an important fact that none of these three precipitation sources can observe or detect the whole rain system or provide sufficient precipitation information. Even though the assimilated precipitation synthesized in this study produced the minimal simulation errors as compared with any of these precipitation products, some precipitation characteristics must have existed, which needs to be explored by specific
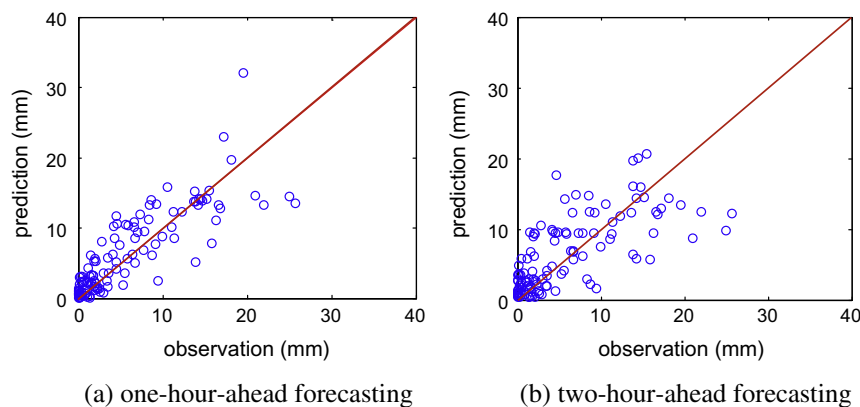

(a) one-hour-ahead forecasting

(b) two-hour-ahead forecasting

Fig. 6. Comparison of observations and (a) one-hour-ahead forecasting as well as (b) two-hour-ahead forecasting obtained from the assimilated precipitation product (A–A module) in the testing phase.

Table 6
Performance of the P–P module-based scenario 1 model, and the improvement made by the scenario 2 model in the testing phase.

	Scenario 1			Scenario 2 (SS)
	Training	Validation	Testing	Testing (%)
t + 1				
CC	0.85	0.82	0.75	14.7
RMSE[a]	4.35	3.77	4.40	25.7
MAE[a]	2.71	2.24	2.81	17.8
t + 2				
CC	0.78	0.76	0.58	22.4
RMSE[a]	5.12	4.23	5.59	19.7
MAE[a]	3.41	2.79	3.91	16.6

[a] Unit (mm/h).

approaches such as the numerical weather analysis. Further investigation of this issue should be another interesting topic and would be of great importance in improving the understanding of real rainfall system.

Fig. 5 illustrates the comparison of ground measurements (blue circle) and the assimilated precipitation in A–A module (histogram), where the gray, green and red bars individually indicate the contribution of the gauge measurements, radar and satellite precipitation products to the assimilated precipitation, respectively. It is clear that both QPESUMS and PERSIANN-CCS information do participate in the merging process even though their contributions are relatively low as compared with gauge measurements. Besides, the contribution of the PERSIANN-CCS is even lower than that of the QPESUMS. It might be because the corrected QPESUMS captured precipitation behavior more accurately than the corrected PERSIANN-CCS (Figs. 3 and 4). Consequently the improvement made by the satellite precipitation product is relatively limited in this study case.

4.3. Rainfall forecasting by ANFIS models

Table 5 shows the rainfall forecasting obtained from the A–A module-based scenarios 1 and 2 by using the ANFIS models and the regression model (scenario 2 only). It clearly shows that the performance of one- and two-hour-ahead rainfall forecast obtained from scenario 2 is more stable in training and testing phases and more accurate (i.e., higher CC values and lower RMSE and MAE values) in all three phases than those of scenario 1. The results suggested that the three individual precipitation inputs (scenario1) might be duplicated and/or controvertible and thus resulted in the propagation of noise and/or conflict information when directly inputting three precipitation sources to the ANFIS, while the composition of the assimilated precipitation might wipe out conflict information and extract merely useful information from different precipitation sources, which not only avoided the problem mentioned above but also reduced the input dimension. Besides, the ANFIS model fed with the assimilated precipitation also provided a better generalization capability. For example, Table 5 shows that the results of scenario 2 for the next hour (*t* + 1) rainfall forecasting maintain similar performance in the training, validation and testing phases (CC > 0.85), whereas the performance of scenario 1 decreases from CC = 0.85 (training) to CC = 0.71 (testing). Similar results can also be found for two-step-ahead (*t* + 2) rainfall forecasts. Moreover, the comparison of the regression-based and the ANFIS-based scenario 2 models show that both methods produced similar results, however the regression method would more commonly underestimate heavy rainfall than the ANFIS and the overall performance of the regression model was slightly worse than that of the ANFIS model. Fig. 6 illustrates the quantitative accuracy of rainfall forecasting for one- and two-hour-ahead forecasting, respectively. It can be found that most of the points are close to the ideal line in each sub-figures, indicating that the rainfall

forecasting performed by the ANFIS is reliable and precise and can be of great help in providing antecedent rainfall information on flood or inundation warnings during typhoon periods.

Table 6 shows the performance of the P–P module-based scenario 1 models for one- and two-step-ahead rainfall forecasting and the corresponding improvement rates made by the scenario 2 models in the testing phase, in terms of CC, RMSE and MAE criteria. It appears that the improvement in rainfall forecasting obtained from scenario 2 greatly increases and the improvement rates in terms of CC, RMSE, and MAE values are about 14.7%, 25.7%, and 17.8% accordingly for the next hour rainfall forecasting, while 22.4%, 19.7%, and 16.6% accordingly for two-hour-ahead rainfall forecasting. Fig. 7 illustrates the performance of the regression-based and the ANFIS-based models (P–P module) for one- and two-hour-ahead rainfall forecasting, respectively. The rainfall pattern of the forecasts obtained from the ANFIS model is relatively close to that of the observations as compared to that of the regression model for one-hour-ahead forecasting (see Fig. 7(a)). For two-hour-ahead rainfall forecasting (see Fig. 7(b)), both models could
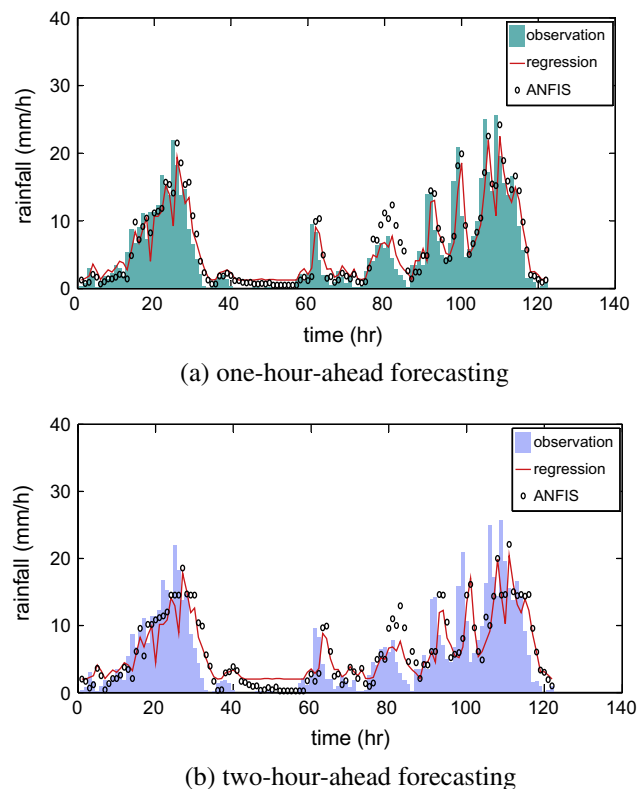

(a) one-hour-ahead forecasting

(b) two-hour-ahead forecasting

Fig. 7. Performance of the regression-based and ANFIS-based models (P–P module) for (a) one-hour-ahead forecasting and (b) two-hour-ahead forecasting in the testing phases.
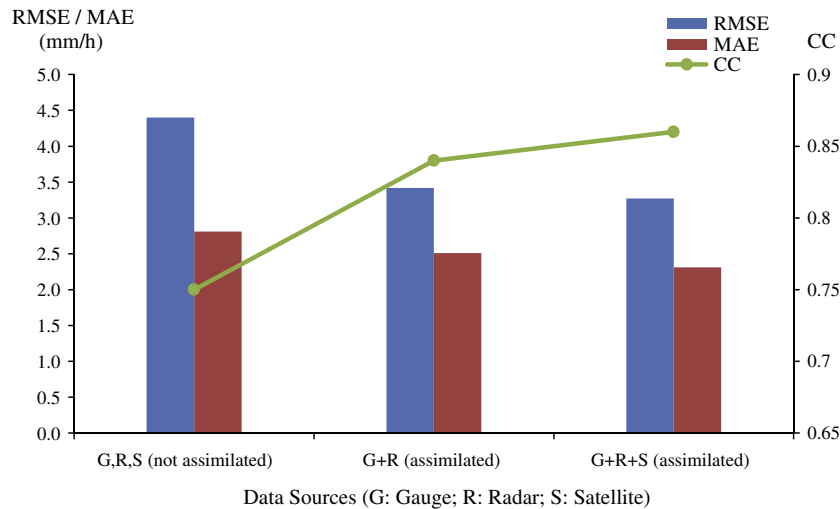
Fig. 8. Comparison of one-hour-ahead forecasting in the testing phases of the ANFIS models with respect to different input combinations of rainfall sources (P–P module).

still capture the main trend and the variation of observations but the effect of time-lag occurred. Overall, these results demonstrate that the thirteen rainfall gauging stations indeed contributed the most to the assimilated precipitation while both QPESUMS- and PERSIANN-CCS-derived precipitation products made certain contributions to the assimilated precipitation, which shows the effectiveness of merging multiple precipitation sources in improving the accuracy and reliability of rainfall forecasting.

To further evaluate the effectiveness of the assimilated precipitation associated with different combinations of precipitation sources, the rainfall forecasting based on the not-assimilated and two assimilated precipitation products is individually performed. Fig. 8 shows the estimation performance of different combinations of rainfall sources (P–P module) in the testing phases of the ANFIS. The results indicate that the model based on the assimilated precipitation of three sources (gauges, radars and satellites) performs the best but the contribution of the satellite precipitation product is less significant to the assimilated precipitation.

5. Conclusions

This study investigated the effectiveness of assimilation-based multi-sensor precipitation estimates (ground gauge measurements, and radar and satellite precipitation products) and made multi-step-ahead rainfall forecasts based on the assimilated precipitation. In the proposed approach, the main tasks: (1) the bias corrections on radar and satellite precipitation products; (2) the assimilation of multi-sensor rainfall sources; and (3) rainfall forecasting, were tackled by a number of applicable and well documented AI techniques. Besides, simple analytical techniques were adopted for ancillary purpose.

For bias corrections, the BPNN was applied to adjusting the biases of the QPESUMS and PERSIANN-CCS according to gauge measurements average precipitation over the basin. Regarding the assimilation of various rainfall sources, two nonlinear search methods (the GA and the LMS) were conducted to search the optimal merging weighting factors for synthesizing the assimilated precipitation. Both GA and LSM produced similar weighting factors and performance. Results reveal that the bias adjustments in QPE-SUMS and PERSIANN-CCS products can significantly improve the accuracy of precipitation products (e.g., 38% improvement for QPE-SUMS; 4% improvements in PERSIANN-CCS in A–A module in the testing phases, in terms of RMSE), and the corrected QPESUMS

and PERSIANN-CCS (in P–P module) individually provide about 24% and 10% contribution to the assimilated precipitation accordingly.

Two input scenarios were implemented to model the one- and two-hour-ahead rainfall forecasting using neural-fuzzy networks. Scenario 1 directly uses all three precipitation information as model inputs, and scenario 2 uses the assimilated precipitation as the only model input. The strategy designed could help to realize the contribution of different precipitation sources to the assimilated precipitation and the improvement in rainfall forecasting obtained from the assimilated precipitation. On the basis of the comparative results, the merging procedure demonstrated its ability to produce more accurate forecasts and better generalization capability for rainfall forecasting during typhoon periods. The evaluation of one- and two-hour-ahead rainfall forecasting schemes strongly shows that the ANFIS model with inputs from scenario 2 provided more accurate and stable rainfall forecasts in comparison with those of scenario 1 and significantly improved the precision of forecasts, for instance, 25% and 19% for one- and two-hour-ahead forecasting accordingly, in terms of RMSE.

Overall, this study gives a detailed and complete investigation on the applicability of the bias adjustments to the QPESUMS and PERSIANN-CCS precipitation products, the corresponding contribution of each precipitation sources to the assimilated precipitation, and the improvement achieved by feeding the estimation models with the assimilated precipitation. The study demonstrates that the ANFIS model can efficiently describe the variation of rainfall and provide reliable one- and two-hour-ahead rainfall forecasts. Moreover, the results also reveal that the bias adjustment and data merging processes proposed in this study are easy but able to provide valuable information for further use, e.g., it helps to increase the accuracy of rainfall forecasting. Such methodology is not confined to locations or weather types but requires streamflow data, rainfall gauge measurements and radar- and satellite-derived precipitation data.

Acknowledgments

References

Adamowski, J., Chan, H.F., 2011. A wavelet neural network conjunction model for groundwater level forecasting. Journal of Hydrology 407, 28–40.

Chang, L.C., Chang, F.J., 2001. Intelligent control for modelling of real-time reservoir operation. Hydrological Processes 15 (9), 1621–1634.

Chang, Y.T., Chang, L.C., Chang, F.J., 2005. Intelligent control for modeling of real-time reservoir operation, Part II: artificial neural network with operating rule curves. Hydrological Processes 19 (7), 1431–1444.

Chen, C.-Y. et al., 2007. Improving debris flow monitoring in Taiwan by using high-resolution rainfall products from QPESUMS. Natural Hazards 40 (2), 447–461.

Chen, S.T., Yu, P.S., Liu, B.W., 2011. Comparison of neural network architectures and inputs for radar rainfall adjustment for typhoon events. Journal of Hydrology 405 (1–2), 150–160.

Chiang, Y.M., Chang, F.J., 2009. Integrating hydrometeorological information for rainfall–runoff modelling by artificial neural networks. Hydrological Processes 23 (11), 1650–1659.

Chiang, Y.M., Chang, L.C., Chang, F.J., 2004. Comparison of static-feedforward and dynamic-feedback neural networks for rainfall–runoff modeling. Journal of Hydrology 290 (3–4), 297–311.

Chiang, Y.M., Hsu, K.L., Chang, F.J., Hong, Y., Sorooshian, S., 2007b. Merging multiple precipitation sources for flash flood forecasting. Journal of Hydrology 340 (3–4), 183–196.

Chiang, Y.M., Chang, F.J., Jou, B.J.D., Lin, P.F., 2007a. Dynamic ANN for precipitation estimation and forecasting from radar observations. Journal of Hydrology 334 (1–2), 250–261.

Chiang, Y.M., Chang, L.C., Tsai, M.J., Wang, Y.F., Chang, F.J., 2010. Dynamic neural networks for real-time water level predictions of sewerage systems-covering gauged and ungauged sites. Hydrology and Earth System Sciences 14 (7), 1309–1319.

Chiang, Y.M., Chang, L.C., Tsai, M.J., Wang, Y.F., Chang, F.J., 2011. Auto-control of pumping operations in sewerage systems by rule-based fuzzy neural networks. Hydrology and Earth System Sciences 15 (1), 185–196.

Chiu, Y.C., Chang, L.C., Chang, F.J., 2007. Using a hybrid genetic algorithm-simulated annealing algorithm for fuzzy programming of reservoir operation. Hydrological Processes 21 (23), 3162–3172.

Coulibaly, P., Evora, N.D., 2007. Comparison of neural network methods for infilling missing daily weather records. Journal of Hydrology 341 (1–2), 27–41.

Firat, M., 2008. Comparison of artificial intelligence techniques for river flow forecasting. Hydrology and Earth System Sciences 12 (1), 123–139.

Grecu, M., Krajewski, W.F., 2000. A large-sample investigation of statistical procedures for radar-based short-term quantitative precipitation forecasting. Journal of Hydrology 239 (1–4), 69–84.

Haiden, T. et al., 2011. The Integrated Nowcasting through Comprehensive Analysis (INCA) system and its validation over the eastern Alpine region. Weather and Forecasting 26 (2), 166–183.

Haykin, S., 1999. Neural Networks, A Comprehensive Foundation. Prentice Hall, Upper Saddle River.

Hong, Y., Hsu, K.L., Sorooshian, S., Gao, X.G., 2004. Precipitation estimation from remotely sensed imagery using an artificial neural network cloud classification system. Journal of Applied Meteorology 43 (12), 1834–1852.

Hong, Y., Hsu, K.L., Sorooshian, S., Gao, X.G., 2005. Self-organizing nonlinear output (SONO): a neural network suitable for cloud patch-based rainfall estimation at small scales. Water Resources Research 41 (3).

Hong, Y., Chiang, Y.M., Liu, Y., Hsu, K.L., Sorooshian, S., 2006. Satellite-based precipitation estimation using watershed segmentation and growing hierarchical self-organizing map. International Journal of Remote Sensing 27 (23–24), 5165–5184.

Jang, J.S.R., 1993. Anfis – adaptive-network-based fuzzy inference system. IEEE Transactions on Systems Man and Cybernetics 23 (3), 665–685.

Juglea, S., Kerr, Y., Mialon, A., Lopez-Baeza, E., Hsu, K., 2010. Soil moisture modelling of a SMOS pixel: interest of using the PERSIANN database over the Valencia Anchor Station. Hydrology and Earth System Sciences 14 (8), 1509–1525.

Kidd, C., Kniveton, D.R., Todd, M.C., Bellerby, T.J., 2003. Satellite rainfall estimation using combined passive microwave and infrared algorithms. Journal of Hydrometeorology 4 (6), 1088–1104.

Kober, K., Craig, G.C., Keil, C., Doernbrack, A., 2012. Blending a probabilistic nowcasting method with a high-resolution numerical weather prediction ensemble for convective precipitation forecasts. Quarterly Journal of the Royal Meteorological Society 138 (664), 755–768.

Kurtulus, B., Razack, M., 2010. Modeling daily discharge responses of a large karstic aquifer using soft computing methods: artificial neural network and neuro-fuzzy. Journal of Hydrology 381 (1–2), 101–111.

Li, M., Shao, Q., 2010. An improved statistical approach to merge satellite rainfall estimates and raingauge data. Journal of Hydrology 385 (1–4), 51–64.

Lohani, A.K., Goel, N.K., Bhatia, K.K.S., 2011. Comparative study of neural network, fuzzy logic and linear transfer function techniques in daily rainfall–runoff modelling under different input domains. Hydrological Processes 25 (2), 175–193.

Mittermaier, M.P., 2008. Introducing uncertainty of radar-rainfall estimates to the verification of mesoscale model precipitation forecasts. Natural Hazards and Earth System Sciences 8 (3), 445–460.

Morin, E., Krajewski, W.F., Goodrich, D.C., Gao, X., Sorooshian, S., 2003. Estimating rainfall intensities from weather radar data: the scale-dependency problem. Journal of Hydrometeorology 4 (5), 782–797.

Shu, C., Ouarda, T.B.M.J., 2008. Regional flood frequency analysis at ungauged sites using the adaptive neuro-fuzzy inference system. Journal of Hydrology 349 (1–2), 31–43.

Siou, L.K.A., Johannet, A., Borrell, V., Pistre, S., 2011. Complexity selection of a neural network model for karst flood forecasting: the case of the Lez Basin (southern France). Journal of Hydrology 403 (3–4), 367–380.

Sokol, Z., 2006. Nowcasting of 1-h precipitation using radar and NWP data. Journal of Hydrology 328 (1–2), 200–211.

Sokol, Z., Pesice, P., 2012. Nowcasting of precipitation–advective statistical forecast model (SAM) for the Czech Republic. Atmospheric Research 103, 70–79.

Yilmaz, A.G., Imteaz, M.A., Jenkins, G., 2011. Catchment flow estimation using artificial neural networks in the mountainous Euphrates Basin. Journal of Hydrology 410 (1–2), 134–140.

Zahraei, A., Hsu, K.L., Sorooshian, S., Gourley, J.J., Lakshmanan, V., Hong, Y., Bellerby, T., 2012. Quantitative precipitation nowcasting: a Lagrangian pixel-based approach. Atmospheric Research 118, 418–434.